AD-A042 669 AIR FORCE INST OF TECH WRIGHT-PATTERSON AFB OHIO F/G 20/11
APPLICATIONS OF THE EXTREMAL PRINCIPLES OF ELASTICITY TO THE DE--ETC(U)
JUL 77 P J TORVIK
UNCLASSIFIED AFIT-TR-77-3 NL

1 OF 1
ADA042 669

END
DATE FILMED
8-77
DDC

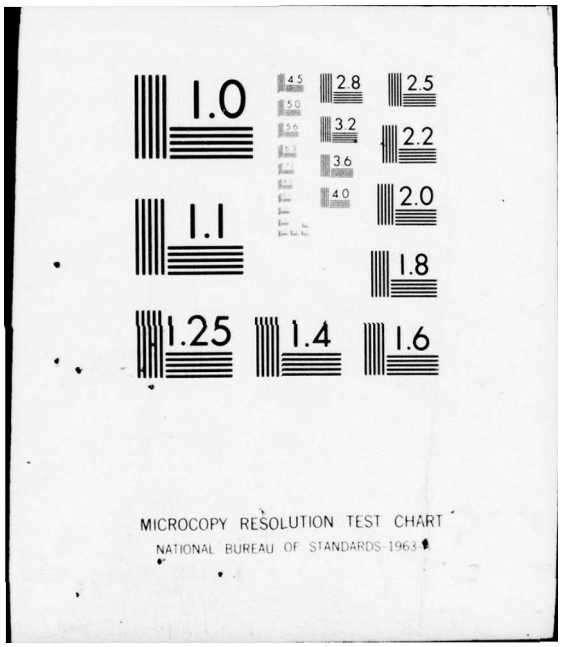
1.0
1.1
1.25
1.4
1.6
1.8
2.0
2.2
2.5
2.8
3.2
3.6
4.0
4.5
5.0
5.6
6.3
MICROCOPY RESOLUTION TEST CHART
NATIONAL BUREAU OF STANDARDS-1963

UNITED STATES AIR FORCE

AIR UNIVERSITY

AIR FORCE INSTITUTE OF TECHNOLOGY

Wright-Patterson Air Force Base, Ohio

APPLICATIONS OF THE EXTREMAL PRINCIPLES OF ELASTICITY TO THE DETERMINATION OF STRESS INTENSITY FACTORS

by

Peter J. Torvik
Professor of Mechanics

AFIT TR 77-3 July 1977

APPLICATIONS OF THE EXTREMAL PRINCIPLES OF ELASTICITY TO THE DETERMINATION OF STRESS INTENSITY FACTORS

BY

Peter J. Torvik
Professor of Mechanics

AFIT TR 77-3

July 1977

UNCLASSIFIED

SECURITY CLASSIFICATION OF THIS PAGE *(When Data Entered)*

REPORT DOCUMENTATION PAGE		READ INSTRUCTIONS BEFORE COMPLETING FORM
1. REPORT NUMBER AFIT-TR-77-3	2. GOVT ACCESSION NO.	3. RECIPIENT'S CATALOG NUMBER
4. TITLE *(and Subtitle)* APPLICATIONS OF THE EXTREMAL PRINCIPLES OF ELASTICITY TO THE DETERMINATION OF STRESS INTENSITY FACTORS.		5. TYPE OF REPORT & PERIOD COVERED Technical Report, 6. PERFORMING ORG. REPORT NUMBER
7. AUTHOR(s) Peter J. Torvik		8. CONTRACT OR GRANT NUMBER(s)
9. PERFORMING ORGANIZATION NAME AND ADDRESS Air Force Institute of Technology Wright-Patterson AFB, Ohio 45433		10. PROGRAM ELEMENT, PROJECT, TASK AREA & WORK UNIT NUMBERS
11. CONTROLLING OFFICE NAME AND ADDRESS Air Force Institute of Technology Wright-Patterson AFB, Ohio 45433		12. REPORT DATE July 1977 13. NUMBER OF PAGES 46
14. MONITORING AGENCY NAME & ADDRESS*(if different from Controlling Office)* 52 p.		15. SECURITY CLASS. *(of this report)* UNCLASSIFIED 15a. DECLASSIFICATION/DOWNGRADING SCHEDULE

16. DISTRIBUTION STATEMENT *(of this Report)*

Approved for public release; distribution unlimited.

17. DISTRIBUTION STATEMENT *(of the abstract entered in Block 20, if different from Report)*

18. SUPPLEMENTARY NOTES

Final Report on AFIT Research
Project No.77-2
April 1977 - July 1977

Approved for public release; IAW AFR 190-17

JERRAL F. GUESS, Captain, USAF
Director of Information

19. KEY WORDS *(Continue on reverse side if necessary and identify by block number)*

Stress Intensity Factors
Fatigue Crack Life Gauge
Energy Methods
Elasticity

20. ABSTRACT *(Continue on reverse side if necessary and identify by block number)*

A method for determining Stress Intensity Factors in edge cracked elastic sheets subjected to arbitrary in-plane loadings is presented. The method employs an eigen-function expansion, with the coefficients chosen through the Energy Principles of Elastostatics. Two-dimensional plane problems with prescribed boundary tractions, prescribed boundary displacement, and mixed problems are considered. Examples given include plates of finite length with edge cracks and plates with cracks originating from the tip of edge notches. Results are given

CONTINUED

DD FORM 1 JAN 73 1473 EDITION OF 1 NOV 65 IS OBSOLETE

012 200

UNCLASSIFIED

SECURITY CLASSIFICATION OF THIS PAGE *(When Data Entered)*

for stress intensity factors in rectangular tensile sheets of various aspect ratios, and for rectangular sheets with prescribed uniform end displacements.

Calibration curves for the Fatigue Crack Life Gauge are developed, and some implications for gauge design are noted.

Table of Contents

		Page
I.	Introduction.	1
II.	Method of Solution.	3
III.	Stress Intensity Factors for Rectangular Sheets in Tension. . .	8
IV.	The Influence of Notches.	16
V.	Mixed Boundary Value Problems	19
VI.	The Rectangular Strip with Prescribed End Displacements	23
VII.	Calibration of the Fatigue Crack Life Gauge	30
VIII.	Discussion and Conclusions.	38

List of Figures

Figure		Page
1	Two-Dimensional Plane Region with Straight Edge Crack. . . .	4
2	Edge-Cracked Rectangular Sheet, Loaded in Tension.	9
3	Stress Intensity Factors for Edge Cracked Plates of Several Aspect Ratios.	12
4	Dependence of Reduced Stress Intensity Factor on Aspect Ratio.	13
5	Cracked Tensile Sheet with Notched Edge.	17
6	Elastic Sheet with Mixed Boundary Conditions	24
7	Rectangular Sheet with Prescribed End Displacements.	25
8	Dimensionless Stress Intensity Factor for Rectangular Plates with Prescribed End Displacements.	27
9	Fatigue Crack Life Gauge	31
10	Dimensionless Crack Tip Displacements.	33
11	Stress Intensity Factors for Fatigue Crack Life Gauges . . .	34

List of Tables

Table		Page
I	Stress Intensity Factors for Edge Cracked Tensile Sheets, $K_I/\sigma_o\sqrt{\pi a}$.	11
II	Convergence of Stress Intensity Factor, $K_I/\sigma_o\sqrt{\pi a}$.	15
III	Dimensionless Stress Intensity Factors for Notched Plates, $K_I/(\sigma_o\sqrt{\pi a})$.	18
IV	Dimensionless Stress Intensity Factor	29

I. Introduction

Various methods[1,2] have been applied to finding stress intensity factors for two dimensional problems in finite regions, including applications of the method of Muskhelishvili, finite element methods, and boundary integral techniques. In addition, there have been several applications of the crack solutions by Williams[3,4] as the elements in a series expansion. The first element in this series contains the square-root singularity in stress. The coefficient of this term is defined to be the stress-intensity factor. The other solutions for the straight crack in the infinite sheet are not singular, but provide a denumerable infinity of solutions of the form $\sigma_{ij}(r,\theta) = r^{n/2-1} f_{ij}(n,\theta)$, $n \geq 2$.

A significant advantage in using the Williams' solutions as elements in an expansion is that each term not only satisfies the field equations, but also satisfies the boundary conditions at points near to the singularity, i.e., on the edges of the crack. Consequently the errors, whether numerical or due to truncation, which result from approximating the boundary conditions on a finite domain are introduced at points well removed from the singularity.

The first applications of the series of Williams' solutions to the finding of stress intensity factors in finite sheets appears to have been made by Gross, Srawley and Brown[5,6,7], in which the necessary coefficients were found by boundary collocation. Stress intensity factors for edge cracked rectangular plates in tension and bending and for other geometries were obtained in this manner. More recently, Hulbert and Hopper[8] determined expansion coefficients by using more boundary points than terms in the series expansion, and determined the coefficients so as to minimize the squared error on the boundary.

In the present work, the Principle of Minimum Potential Energy is used to develop an algorithm for finding the appropriate coefficients of an expansion for stresses and displacements when an arbitrary in-plane traction is applied at the circumference of an arbitrary, edge-cracked, finite domain. It is also shown that the Principle of Minimum Complementary Energy, together with the series of Williams' solutions, is appropriate when displacements are prescribed on the edge of the plate. Finally, Reissner's Principle is used to find the coefficients of the expansion when displacements are given on some portion of the boundary, and tractions are prescribed on the remainder.

II. Method of Solution

The region of interest is depicted graphically as Figure 1. A simply connected elastic sheet of negligible thickness (plane stress) is assumed to contain a straight crack of length a, originating at an edge. For convenience, an origin of coordinates is placed at the crack tip, with crack boundaries S_1 and S_3 located at $\theta = \pm \pi$, $0 \leq r \leq a$. In-plane tractions are assumed to be prescribed on the curve S, with values prescribed to be zero on S_1 and S_3.

It has been shown by Williams[3,4] that the equations of elastostatics are satisfied for the infinite domain by stress functions of the form

$$\chi(r,\theta,\lambda) \equiv r^{\lambda+1} F(\theta;\lambda) \tag{1}$$

For the crack, the eigenvalues λ are $\lambda = m/2$, for all integers m. For the coordinates shown, the stress function may be divided, for convenience, into an even and an odd part. The even stress function and the corresponding infinite set of stresses are given in Appendix I. For each n there are two states of stress, each of which is multiplied by an arbitrary coefficient and each of which satisfies the field equations and the traction free boundary condition on the crack edges. For simplicity in that which follows, let us designate a superposition of M of these solutions as:

$$\begin{bmatrix} \sigma_{rr} \\ \sigma_{\theta\theta} \\ \sigma_{r\theta} \end{bmatrix} = \sum_{m=1}^{M} d_m \cdot \begin{bmatrix} \sigma_{rr}^{m} \\ \sigma_{\theta\theta}^{m} \\ \sigma_{r\theta}^{m} \end{bmatrix} \tag{2}$$

where $d_1 = a_1$, $d_2 = -a_2$, $d_3 = -a_3$, $d_4 = a_4$, etc.

Our purpose, then, is to develop an efficient algorithm for finding the set of M coefficients which give the best approximation to the stresses within an arbitrary finite domain, using the first M eigenfunctions. As

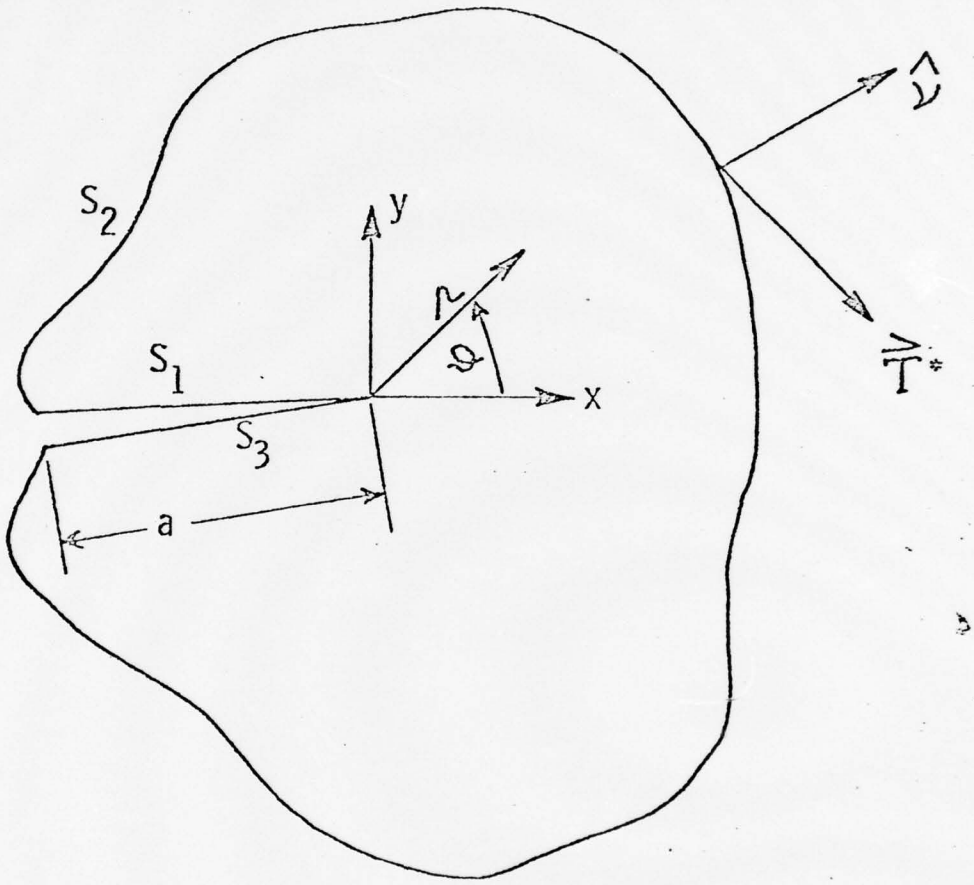

Figure 1 Two-Dimensional Plane Region with Straight Edge Crack

noted earlier, both collocation and the method of least squares have been used for this purpose. Here, we seek to use an extremal principle of elastostatics.

As was shown by Williams[3,4], displacements corresponding to each term in the stress function may be found through

$$2\mu\, u_r = \frac{-\partial \chi}{\partial r} + (1-\sigma) r \frac{\partial \psi}{\partial \theta} \tag{3}$$

$$2\mu\, u_\theta = -\frac{1}{r}\frac{\partial \chi}{\partial \theta} + (1-\sigma) r^2 \frac{\partial \psi}{\partial r}$$

where μ is the shear modulus, ν is Poisson's ratio, σ is taken to be ν for plane strain, and $\sigma = \nu/(1+\nu)$ in the case of plane stress. The function ψ which corresponds to the even stress function and the resulting displacements are given in the appendix.

Thus, for any m we have a set of displacements, u_r^m, u_θ^m which, upon application of the strain displacement equations and the stress strain laws, will yield the stresses σ_{rr}^m, $\sigma_{\theta\theta}^m$ and $\sigma_{r\theta}^m$. For the class of problems with prescribed tractions $\vec{T}^*$ on the boundary, these displacements are kinetically admissable, as is the superposition,

$$\begin{bmatrix} 2\mu\, u_r \\ 2\mu\, u_\theta \end{bmatrix} = \sum_{m=1}^{M} d_m \cdot \begin{bmatrix} u_r^m \\ u_\theta^m \end{bmatrix} \tag{5}$$

Such displacements are therefore appropriate for use in the Principle of Minimum Potential Energy[9], with the d_m to be chosen to achieve the minimum. Let

$$\pi = \iiint_V W(u_i)dv - \iiint_V F_i u_i dv - \iint_{S_T} T_i^* u_i dS \tag{6}$$

where

W is the strain energy density

F_i are body forces and

T_i^* are tractions, prescribed on S_T.

In the present work, the body forces are zero, and S_T is the entire contour. Taking the first variation yields, after some manipulation, that

$$\delta \pi = 0 = \iint_{S_T} (T_i - T_i^*)\, \delta u_i \, ds \tag{7}$$

Use has been made of the fact that

$$\frac{\partial}{\partial x_j}\left(\frac{\partial W}{\partial \varepsilon_{ij}}\right) = 0 \tag{8}$$

since, by construction, the stresses arising from the kinematically admissable displacements satisfy the equilibrium equations.

For displacements as given by Equation 5, the variations are

$$\begin{bmatrix} 2\mu\delta\, u_r \\ 2\mu\delta\, u_\theta \end{bmatrix} = \sum_{p=1}^{M} \delta d_p \cdot \begin{bmatrix} u_r^p \\ u_\theta^p \end{bmatrix} \tag{9}$$

Writing the traction vector and the unit outward normal at any point on S_T in terms of components, Equation 7 becomes

$$\int_{S_T} \left(\nu_r \sum_{m=1}^{M} d_m \sigma_{rr}^m + \nu_\theta \sum_{m=1}^{M} d_m \sigma_{\theta r}^m\right) - T_r^* \sum_{p=1}^{M} \delta d_p u_r^p \tag{10}$$

$$+ \int_{S_T} \left(\nu_r \sum_{m=1}^{M} d_m \sigma_{r\theta}^m + \nu_\theta \sum_{m=1}^{M} d_m \sigma_{\theta\theta}^m - T_\theta^*\right) \sum_{p=1}^{M} \delta d_p u_\theta^p = 0$$

Since the variations must be arbitrary, Equation 10 must be satisfied for any choice of δd_p. In particular, it must be satisfied for the selection

$$\delta d_p = 0 \text{ if } p \neq q\,, \quad \delta d_p = 1 \text{ if } p = q\,. \tag{11}$$

Thus,

$$\sum_{m=1}^{M} d_m C_{mq} = D_q \tag{12}$$

$$C_{mq} = \int_{S_T} \{(\nu_r \sigma_{rr}{}^m + \nu_\theta \sigma_{\theta r}{}^m) u_r{}^q + (\nu_r \sigma_{r\theta}{}^m + \nu_\theta \sigma_{\theta\theta}{}^m) u_\theta{}^q\} ds \qquad (13)$$

$$D_q = \int_{S_T} \{T_r{}^*(r,\theta) u_r{}^q + T_\theta{}^*(r,\theta) u_\theta{}^q\} ds \qquad (14)$$

The desired algorithm for choosing the coefficients d_m has now been obtained. For any preselected number of terms, M, to be used in the expansion, the elements of the square array C_{mq} (which can be shown to be symmetric) are evaluated. The prescribed tractions are substituted into Equation 14, and the M vector D_q is computed. Post-multiplying by C^{-1} leads to the coefficients d_m.

For purposes of determining stress intensity factors, it is the first of these coefficients which is of interest. Let

$$K_I = \lim_{r \to 0} \{ \sqrt{2\pi r}\ \sigma_{\theta\theta}(\theta=0,r) \} \qquad (15)$$

Only the first term survives the limit process, thus

$$K_I = - \sqrt{2\pi}\ a_1 = - \sqrt{2\pi}\ d_1 \qquad (16)$$

The coefficients d_m will have a linear dependence on the far field stress, through Equations 12 and 14, thus the results may be put into the usual dimensionless form for the Mode I stress intensity factor, through

$$\frac{K_I}{\sigma_o \sqrt{\pi a}} = - \sqrt{\frac{2}{a}} \frac{d_1}{\sigma_o} \qquad (17)$$

where a is the crack length, and σ_o is a suitable measure of the far-field stress.

III. Stress Intensity Factors for Rectangular Sheets in Tension

The rectangular sheet with edge crack loaded in uniaxial tension was selected as a suitable problem for verifying the feasibility of the method. The problem is of considerable interest; consequently, previously obtained results are available for comparison.

We consider a rectangular sheet of length L and width b, subjected to a uniform traction T_y of magnitude σ_o and no shear on the ends, the other faces being free. The geometry of the problem is depicted in Figure 2. For this simply connected problem with traction boundary conditions, the exact solution should be independent of Poisson's ratio. However, the present method introduces Poisson's ratio through the displacements. A value of $\nu = 0.3$ was used in the calculations here reported.

Since each of the stresses $\sigma_{\theta\theta}^{m}$ and $\sigma_{r\theta}^{m}$ vanishes on $\theta = \pm \pi$, integration over that portion of the boundary produces no contributions to the matrix defined by Equation 13. For the problem at hand, the tractions on C_1 and C_3 are prescribed to be zero, thus the vector D_q is computed by integration over C_2 only. In this symmetric problem, only the upper half plane need be considered. Since the boundary tractions on the plane $y = L/2$ are prescribed in the Cartesian frame, the computation of the invariant quantity

$$D_q = \int_{C_2} \vec{T}^{*} \cdot \vec{u}^{q} \, ds \tag{18}$$

is more conveniently performed in the Cartesian system, i.e.,

$$D_q = \int_{x=-a}^{x=b-a} T_x^{*}(u_r^{q} \cos\theta - u_\theta^{q} \sin\theta) + T_y^{*}(u_r^{q} \sin\theta + u_\theta^{q} \cos\theta)\,dx \tag{19}$$

Here, $T_x^{*} = 0$ and $T_y^{*} = \sigma_o$.

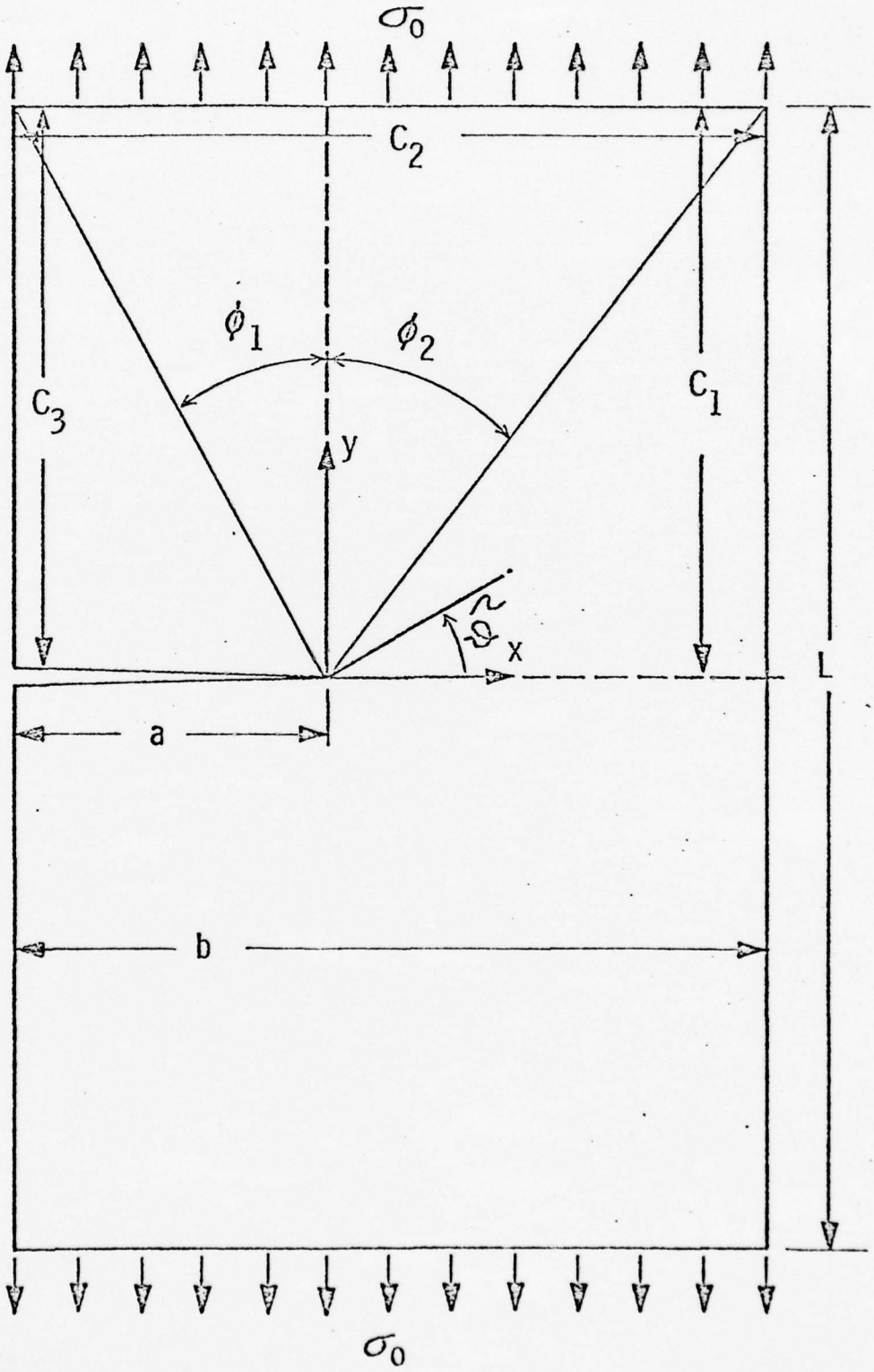

Figure 2 Edge-Cracked Rectangular Sheet, Loaded in Tension

Since evaluation of the integrals in Equations 13 and 14 in closed form is not feasible for the geometry selected, and certainly not for more complex shapes, a numerical integration using Simpson's rule was employed. Division of the boundary curve $C_1 + C_2 + C_3$ into 200-400 points was found to be sufficient to keep the results insensitive to the number of points used. The approximations introduced through these numerical integrations appeared to place a limit on the crack depths which can be considered by this method. Sensitivity to the number of integration points began to appear when the distance from the crack tip to the nearest boundary was allowed to become less than about ten times the distance between integration points. As a practical matter, this limitation is of no consequence, for the available closed form solutions[10] for very shallow and very deep cracks in strips of infinite length are applicable to such geometries.

Selected values of the Mode I Stress Intensity Factor are tabulated in Table I for various crack lengths and aspect ratios. A graphical comparison of some of these results is given as Figure 3. The form used by Tada[11] was found to be particularly convenient for this comparison. The use of a dimensionless factor, N, defined through

$$N(a/b, L/b) = \frac{K_I(a/b, L/b)}{\sigma_o \sqrt{\pi a}} (1 - a/b)^{3/2} \qquad (20)$$

was found to reduce the large variations evident in Figure 3 to the more readily useable results presented as Figure 4.

Numerical values obtained at small a/b (0.05 to 0.10) appear to converge satisfactorily[10] to the known value for $a/b \to o$, as do the numerical values obtained at large a/b (0.9 to 0.95). Values of N obtained for large L/b (L/b = 2, 3 and 4) give satisfactory agreement with the curve presented by Tada[11] as a composite of previously obtained values for long

Table I.

Stress Intensity Factors for Edge Cracked Tensile Sheets, $K_I/\sigma_o\sqrt{\pi a}$

a/b	L/b = 4	L/b = 3	L/b = 2	L/b = 1	L/b = .75	L/b = .5
.1	1.23*	1.21	1.20	1.23	1.30	1.48
.2	1.37	1.37	1.37	1.49	1.68	2.15
.3	1.66	1.66	1.66	1.85	2.16	2.95
.4	2.11	2.11	2.11	2.32	2.72	3.84
.5	2.82	2.82	2.83	3.01	3.42	4.81
.6	4.00	4.02	4.03	4.15	4.49	5.94
.7	6.25	6.29	6.34	6.39	6.58	7.73
.8	11.6 *	11.3	11.8	11.9	12.0	12.5
.9				32.9	34.3	34.3

*-Denotes Uncertainty in 3rd Digit

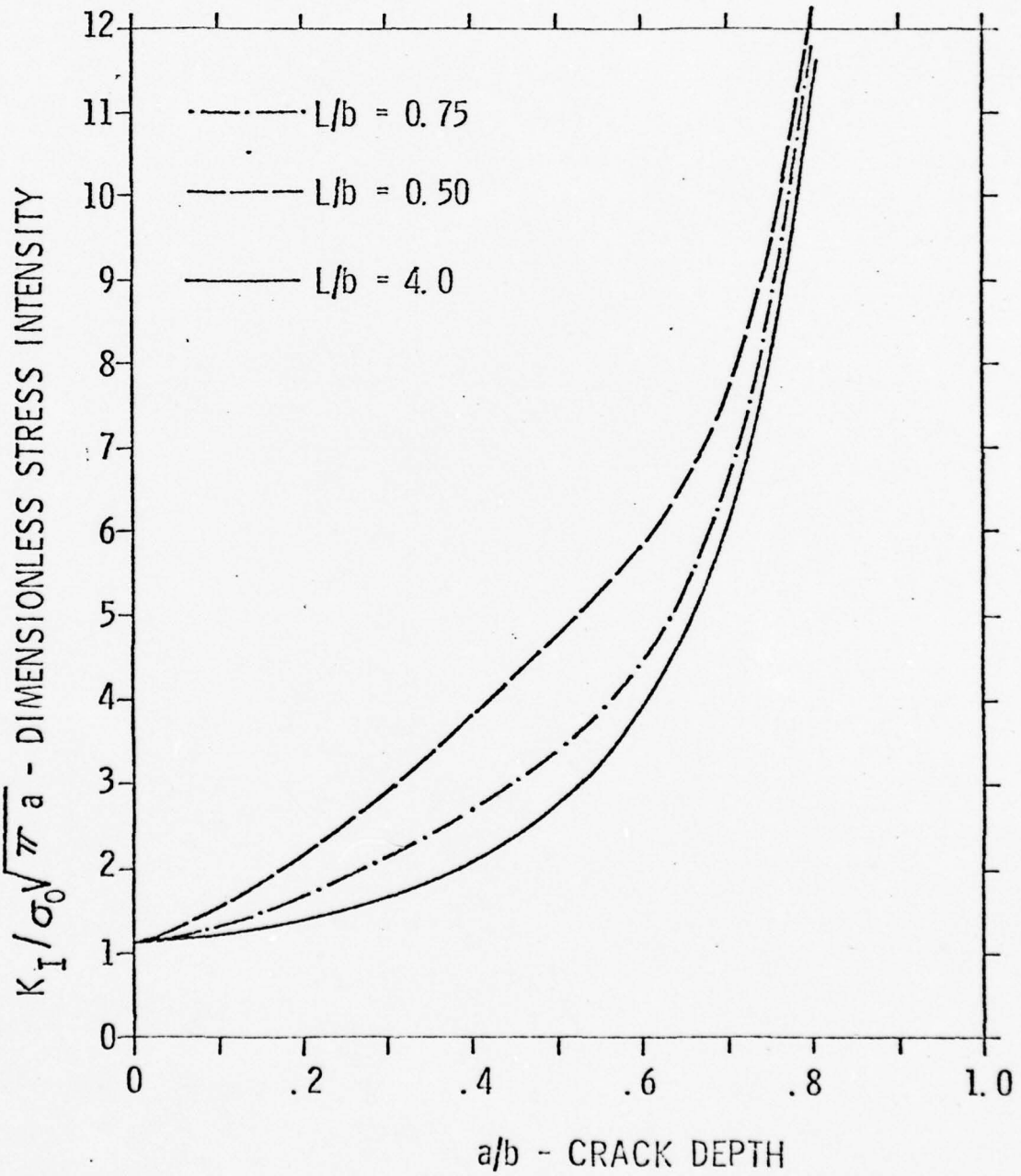

Figure 3 Stress Intensity Factors for Edge Cracked Plates of Several Aspect Ratios

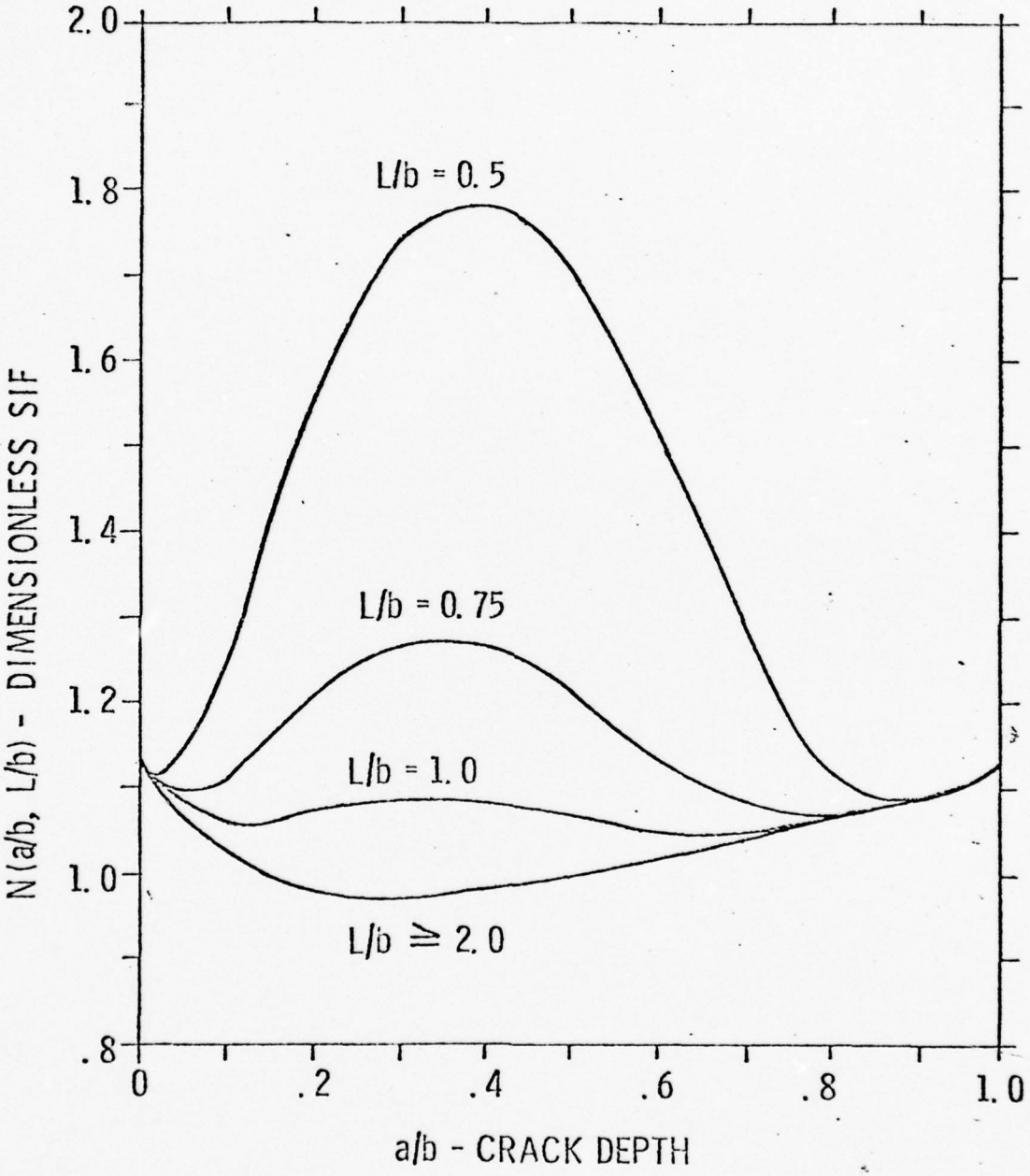

Figure 4 Dependence of Reduced Stress Intensity Factor on Aspect Ratio

and infinite strips by Bowie and Neal[12], Emery and Segedin[13], and others.

Expansions using from eight to 48 terms were investigated. In most cases, 24 to 36 terms were found adequate to give convergence to three significant digits in the value of the first coefficient. More terms were generally required for good convergence as the ratio L/b was made large and as the crack depth approached the plate edge. From results such as those given in Table II, it is suggested that convergence in the third significant figure will only be achieved if the most rapidly oscillating term has half period less than the smaller of ϕ_1 and ϕ_2 (Figure 2), i.e., $M\phi \geq 2\pi$. Some evidence of numerical difficulty began to appear in 48 term expansions. These were attributed to the large variations between the magnitudes of the elements of the C matrix which occurs in such cases. Thus, the method is not well suited to extremely long strips. This again is of no consequence, as results for such geometries are readily obtained by using the known results for the infinite strip and St. Venant's Principle.

The determination of a single set of coefficients on a CDC 6600 computer with a program which was not particularly efficient was found to require a run time of approximately $0.3M^2N_p \times 10^{03}$ sec, where N_p is the number of boundary points used for the numerical integration.

Table II

Convergence of Stress Intensity Factor, $K_I/\sigma_o\sqrt{\pi a}$

	M = 8	M = 16	M = 24	M = 32	M = 36
L/b = 1, a/b = 0.1	1.345	1.242	1.238	1.232	1.228
L/b = 1, a/b = 0.2	1.496	1.490	1.489	1.486	1.486
L/b = 1, a/b = 0.5	2.898	3.134	3.009	3.009	3.009
L/b = 1, a/b = 0.8	8.743	11.35	11.85	11.93	11.94
L/b = 4, a/b = 0.5	2.215	2.653	2.738	2.814	2.820

IV. The Influence of Notches

The applicability of the procedure here presented to complex boundaries was used to investigate, in a limited manner, the influence of notch width on the stress intensity factor for cracks originating from the notch root. The geometry considered is shown in Figure 5. A triangular notch of depth d and width 2h is assumed to be machined into the edge of a rectangular tensile sheet of width b and length L. A straight crack of length a-d is assumed to originate at the notch root. For h = 0, the problem reduces to that of an edge crack of depth a. The numerical integration in Equation 13 was accomplished by dividing the boundary segment C_3 into two segments, AB and BC. Since the notch faces are free of traction, no change in the vector D_q results.

Numerical results were obtained for a square plate (L/b = 1) with notch depth d/b = 0.25. The distance, a, from the edge of the plate to the crack tip was varied from a/b = .3 to a/b = .5. Dimensionless stress intensity factors are compared in Table III for several notch widths. It is evident from the results that notches have little effect on the stress intensity factor once the crack is well established ($a_c/d \geq 0.2$). Thus, it is to be concluded that the practice employed in experimental work of using a narrow machined cut as a crack starter and then considering the depth of cut to be a portion of the crack is not a source of significant error.

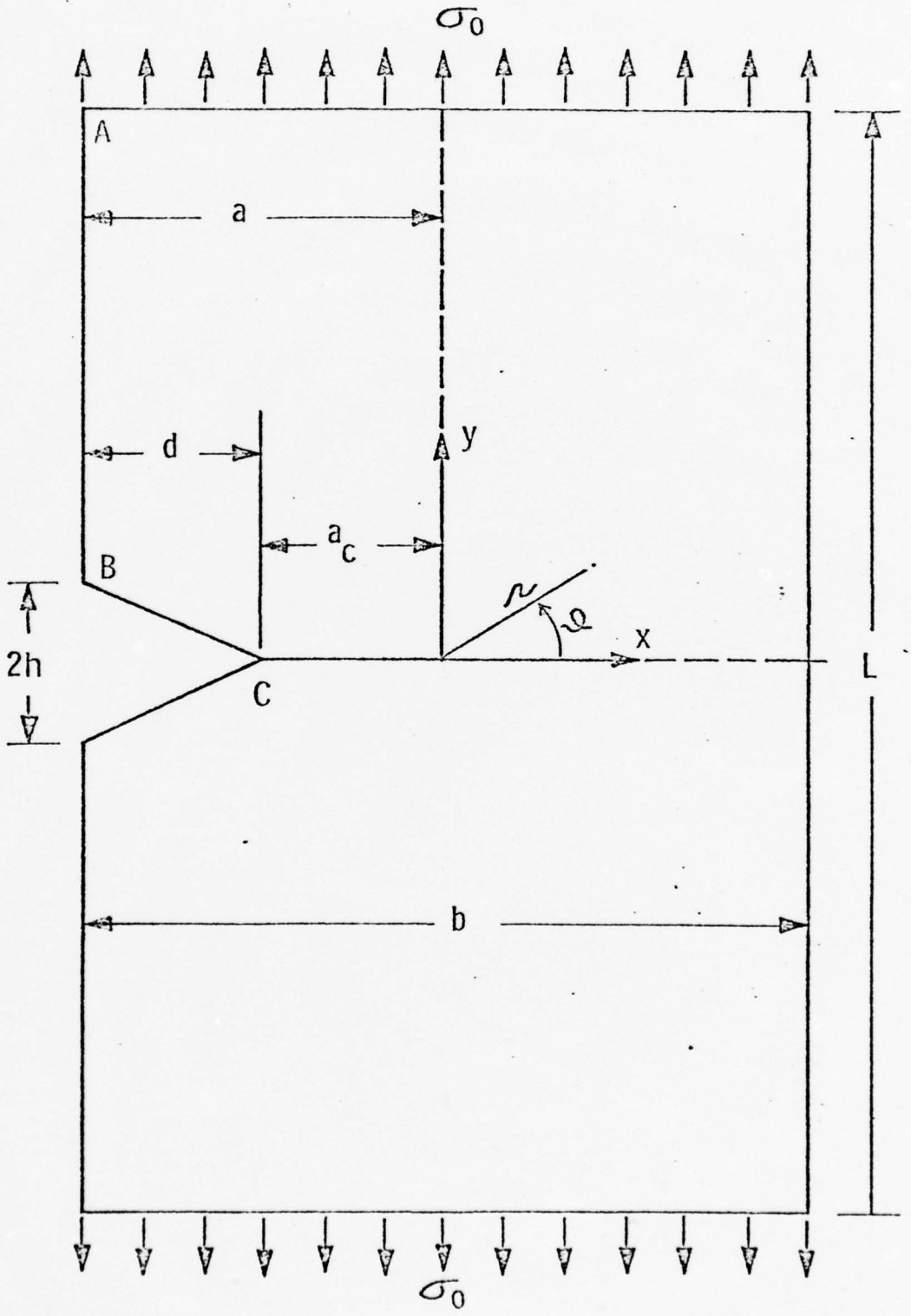

Figure 5 Cracked Tensile Sheet with Notched Edge

Table III

Dimensionless Stress Intensity Factors

for Notched Plates, $K_I/(\sigma_o\sqrt{\pi a})$

	a/b				
2h/L	0.3	0.35	0.4	0.45	0.5
0	1.85	2.07	2.32	2.63	3.01
.1	1.85	2.07	2.32	2.63	3.01
.5	1.86	2.07	2.33	2.63	3.01
1.0	1.85	2.07	2.33	2.64	3.02

V. Mixed Boundary Value Problems

If displacements, $\vec{u}^*$, rather than stresses, are prescribed on the boundary S_2 (Figure 1) and the tractions are prescribed to be zero on S_1 and S_3, as before, a mixed boundary value problem results. For such problems, each of the Williams' solutions is a statically admissable system of stresses since each satisfies equilibrium and the traction boundary conditions. Thus, any superposition, such as Equation 2, is also statically admissable and may be used in the Principle of Minimum Complementary Energy[9].

$$\pi^* = \iiint_V W_c(\sigma_{ij})dV - \iint_{S_u} \vec{u}^* \cdot \vec{T}\, ds \tag{21}$$

The variation of π^* is taken, with the stresses treated as the independent variables. Variations of the stresses,

$$\delta\sigma_{ij} = \sum_{p=1}^{M} \delta d_p \sigma_{ij}{}^p \tag{22}$$

satisfy the equilibrium equations and the traction free condition on S_1+S_3. Thus, setting the first variation of the Complementary Energy to zero leads to

$$\int_{S_2} \{2\mu u_i{}^* - \sum_{m=1}^{M} d_m u_i{}^m\} \cdot \sum_{p=1}^{M} \delta d_p \nu_j \sigma_{ji}{}^p ds = 0 \tag{23}$$

The same choice of variation coefficients as given in Equation 11 is apropos; thus the algorithm for determining the coefficients of the expansion is seen to be

$$\sum_{m=1}^{M} d_m B_{mq} = E_q \tag{24}$$

where

$$B_{mq} = \int_{S_2} \nu_j u_i{}^m \sigma_{ji}{}^q ds \tag{25}$$

$$E_q = \int_{S_2} 2\mu\, u_i{}^* \nu_j \sigma_{ji}{}^q ds \tag{26}$$

One complication arises in this mixed problem which is not present when tractions alone are prescribed. Each term in the expansion can be seen (Appendix I) to have zero displacement at the origin of coordinates. Thus, the crack tip is automatically specified to be a fixed point. When tractions are prescribed on S this is of no consequence, and serves to remove the rigid body displacements. When displacements are to be specified on some portion of S, however, the crack tip must be left free to translate. This may be accomplished by including the two possible rigid body displacements as additional elements of the expansion. These solutions, in polar coordinates, are

$$\begin{aligned} 2\mu\, u_r &= d_o\, u_r^o = d_o \cos\theta \\ 2\mu\, u_\theta &= d_o\, u_\theta^o = -d_o \sin\theta \end{aligned} \tag{27}$$

for x axis translation, and

$$\begin{aligned} 2\mu\, u_r &= d_{-1} u_r^o = d_{-1} \sin\theta \\ 2\mu\, u_\theta &= d_{-1} u_\theta^o = d_{-1} \cos\theta \end{aligned} \tag{28}$$

for y axis translation. Of these, only the former (Equation 27) is symmetric with respect to the x axis and appropriate for inclusion with the symmetric solutions given in the appendix. This solution represents a rigid body motion; thus the corresponding stresses, σ_{rr}^o, $\sigma_{r\theta}^o$ and $\sigma_{\theta\theta}^o$, all vanish.

A more interesting class of problems arises if the boundary S_2 (Figure 1) is allowed to be divided into two regions, C_T and C_u, with tractions prescribed on C_T and displacements on C_u. Neither the Principle of Minimum Potential Energy nor the Principle of Minimum Complementary Energy can be applied to such problems, for the Williams' solutions are then neither statically admissable nor kinematically admissable. It will be shown, however, that Reissner's Principle[9] can be used to develop an algorithm for

determining the desired set of coefficients.

We consider the functional

$$J = \int_V \{W(\varepsilon_{ij}) - F_i u_i\} dV - \int_V \sigma_{ij}\{\varepsilon_{ij} - \frac{1}{2}(u_{i,j} + u_{j,i})\} dV \tag{29}$$

$$- \int_{S_T} T_i^* \cdot u_i ds - \int_{S_u} T_i (u_i - u_i^*) ds$$

where $S_u \equiv C_u$ and $S_T = C_T + S_1 + S_3$, and consider stresses, strains and displacements all to be independent variables. We let the displacements be given by Equation 5, the stresses by Equations 2, and the strains by an analagous form. Each element of the expansion then satisfies the equilibrium equations, the strain displacement equations, and Hookes' law. Setting the first variation to zero leads to

$$\delta J = 0 = \int_S T_i \cdot \delta u_i ds - \int_{S_T} T_i^* \cdot \delta u_i ds - \int_{S_u} \delta T_i \cdot (u_i - u_i^*) ds \tag{30}$$

$$- \int_{S_u} T_i \delta u_i ds$$

or

$$0 = \int_{C_T} (T_i - T_i^*) \cdot \delta u_i ds - \int_{C_u} \delta T_i \cdot (u_i - u_i^*) ds \tag{31}$$

Since $T_i = T_i^* = 0$ on $S_T - C_T = S_1 + S_3$ for each element of the expansion. Substituting Equations 9 and 22, and making the same choice of variation coefficients as specified by Equation 11, we find that the desired expression for the expansion coefficients is

$$\int_{C_T} \nu_j \sum_{m=1}^{M} d_m \sigma_{ji}^m u_i^q ds - \int_{C_u} \nu_j \sigma_{ji}^q \sum_{m=1}^{M} d_m u_i^m ds = \int_{C_T} T_i^* u_i^q ds - \int_{C_u} 2\mu\, u_i^* \nu_j \sigma_{ji}^q ds \tag{32}$$

$$\sum_{m=1}^{M} d_m A_{mq} = F_q = D_q - E_q \tag{33}$$

where

$$A_{mq} = \int_{C_T} \nu_j \sigma_{ji}{}^{m} u_i{}^{q} ds - \int_{C_u} \nu_j \sigma_{ji}{}^{q} u_i{}^{m} ds \qquad (34)$$

If $C_u \to o$, Equation 12 is recovered; if $C_T \to o$, Equation 24 results.

VI. The Rectangular Strip with Prescribed End Displacements

The method developed in the preceeding section for determining coefficients for displacements and stresses expressed as a series of Williams' solutions can be applied to the determination of stress intensity factors for the rectangular sheet with two free edges, prescribed end displacement, and an edge crack. This problem has been considered previously by Bowie[14], who used a conformal mapping, and by Bradley and Kobayashi[15], who have fit several terms from the Williams' solutions to data obtained from photoelastic experiments. The geometry of interest is shown in Figure 6. Surfaces S_1, C_{T_1}, and C_{T_2} are free of traction and displacements are prescribed on C_{u_1}. For this symmetric geometry, and for symmetric loadings, i.e.,

$$u_y(x,L/2) = -u_y(x,-L/2); \quad u_x(x,L/2) = u_x(x,-L/2) \tag{35}$$

only the upper half plane need be considered. Thus,

$$A_{mq} = \int_{C_{T_1}+C_{T_2}} \{\nu_r\sigma_{rr}{}^m + \nu_\theta\sigma_{\theta r}{}^m)u_r{}^q + (\nu_r\sigma_{r\theta}{}^m + \nu_\theta\sigma_{\theta\theta}{}^m)u_\theta{}^q\}ds$$
$$- \int_{C_{u_1}} \{(\nu_r\sigma_{rr}{}^q + \nu_\theta\sigma_{\theta r}{}^q)u_r{}^m + (\nu_r\sigma_{r\theta}{}^q + \nu_\theta\sigma_{\theta\theta}{}^q)u_\theta{}^m\}ds \tag{36}$$

$$F_q = -2\mu \int_{C_{u_1}} \{(u_x{}^*\cos\theta + u_y{}^*\sin\theta)(\nu_r\sigma_{rr}{}^q + \nu_\theta\sigma_{\theta r}{}^q)$$
$$+ (-u_x{}^*\sin\theta + u_y{}^*\cos\theta)(\nu_r\sigma_{r\theta}{}^q + \nu_\theta\sigma_{\theta\theta}{}^q)\}ds \tag{37}$$

and the d_m are obtained from Equation 33.

Numerical results were obtained for a uniform extension with no transverse displacements on the ends of a sheet of length L and width b, having an edge crack of length a. The geometry is shown in Figure 7. The

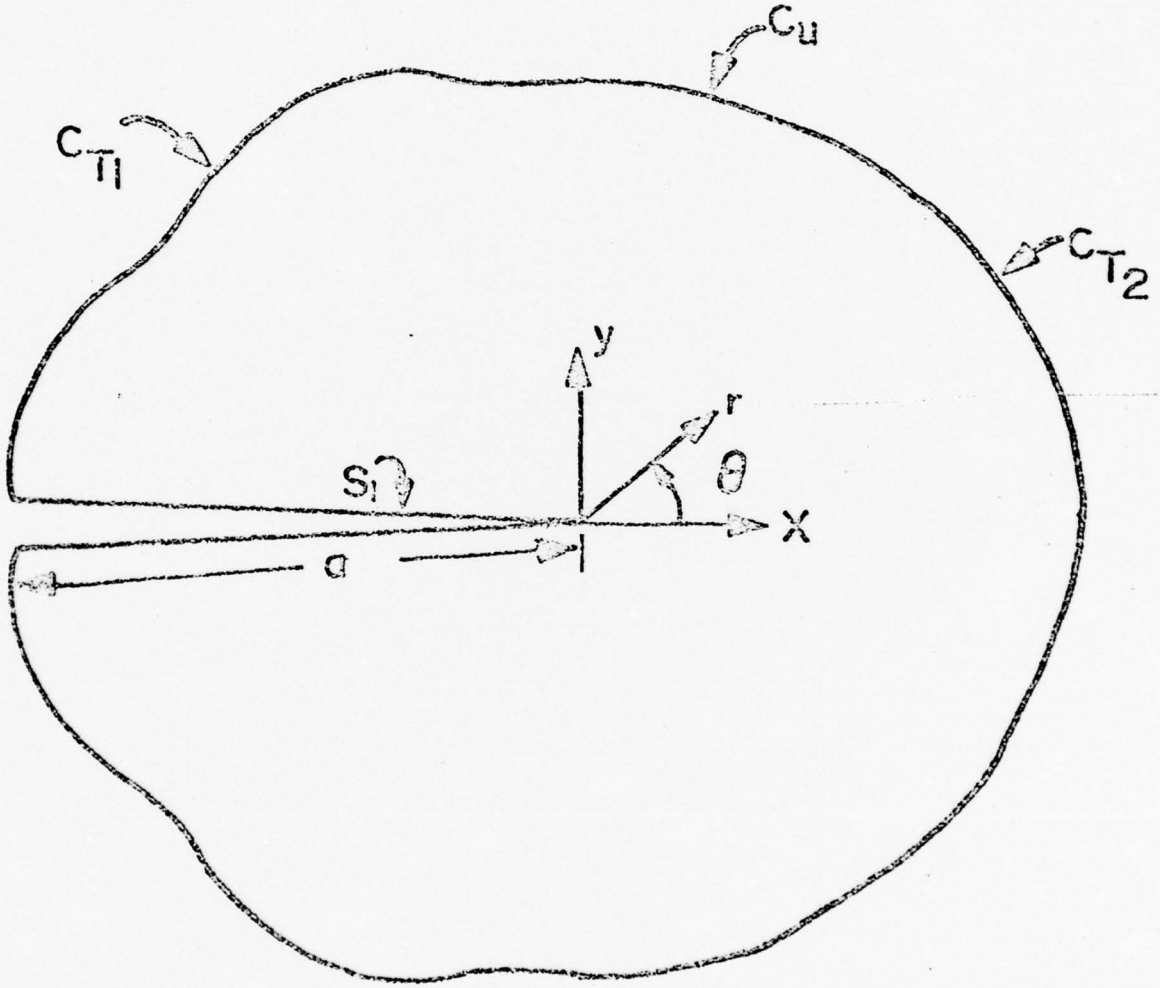

Figure 6 Elastic Sheet with Mixed Boundary Conditions

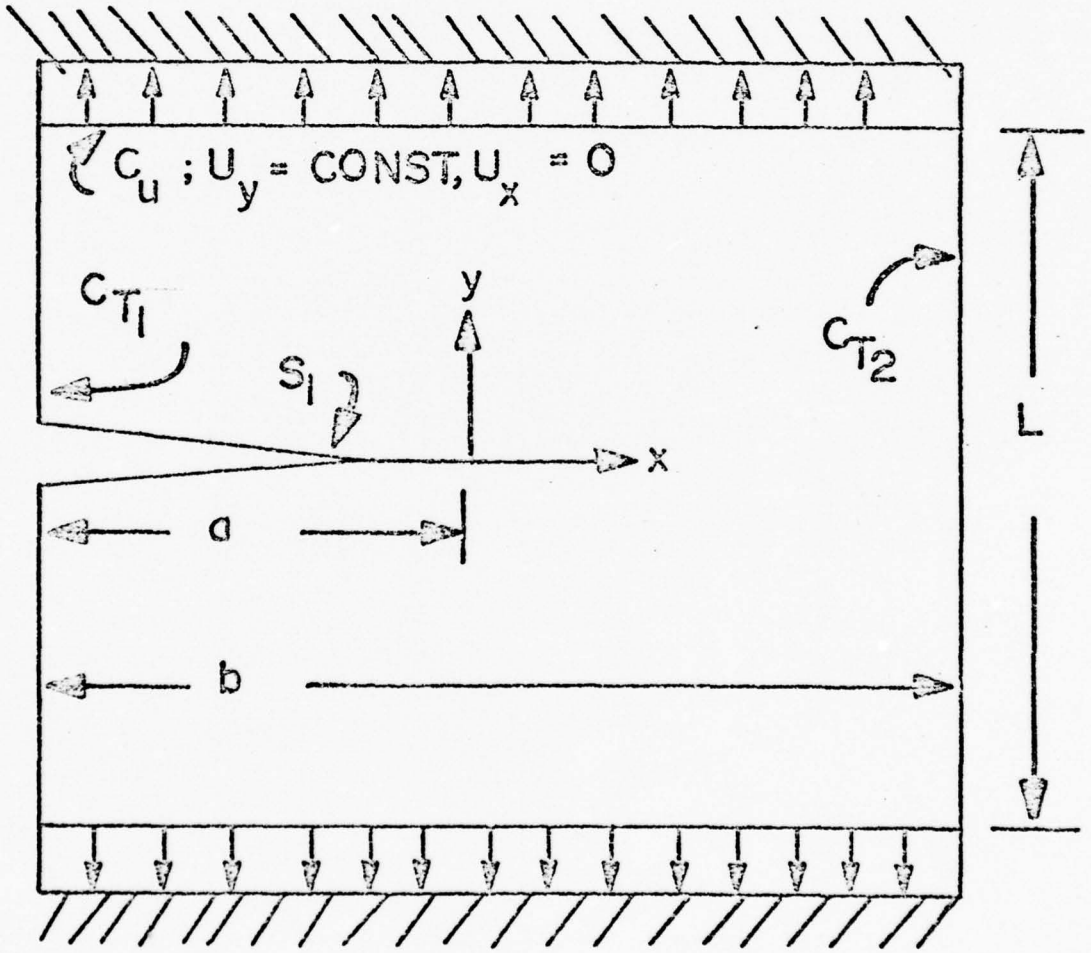

Figure 7 Rectangular Sheet with Prescribed End Displacements

prescribed displacements are:

$$u_y(x,L/2) = u_y^* \text{ and}$$
$$u_x(x,L/2) = 0 \tag{38}$$

Results were obtained by using 34 of the Williams' solutions and the rigid body mode previously discussed as the elements of the expansion. The numerical integration was found to require 300-400 points on the boundary. Convergence of the numerical solution was found to be similar to that previously discussed for prescribed boundary tractions.

A convenient means of reducing the Mode I Stress Intensity Factor to a dimensionless form is through division by $\sigma_o\sqrt{\pi a}$, where

$$\sigma_o = \frac{E}{1-\nu^2}\left(\frac{2u_y^*}{L}\right) \tag{39}$$

is the uniform traction which must be applied on $y = \pm L/2$ in order to produce the same displacements in an uncracked sheet of the same material, subject to complete transverse constraint, $\varepsilon_{xx} = 0$. Thus

$$\frac{K_I}{\sigma_o\sqrt{\pi a}} = \frac{K_I}{\frac{E}{1-\nu^2}\left(\frac{2u_y^*}{L}\right)\sqrt{\pi a}} = (1-\nu^2)\sqrt{\frac{2}{a}}\,(-d_1) \tag{40}$$

Numerical results for several aspect ratios are presented as the dashed curves of Figure 8 for the case $\nu = 0.3$.

The results obtained for $L/b = 1.0$ appear to be in good agreement with those plotted by Bradley and Kobayaski[15]. The present results can also be compared with the exact result for a limiting case. For an elastic strip of infinite width, having displacements u_y^* on clamped edges at $y = \pm L/2$, Rice[16] has shown the stress intensity factor to be

$$K_I = E\,u_y^*\sqrt{\frac{2}{L(1-\nu^2)}} \tag{41}$$

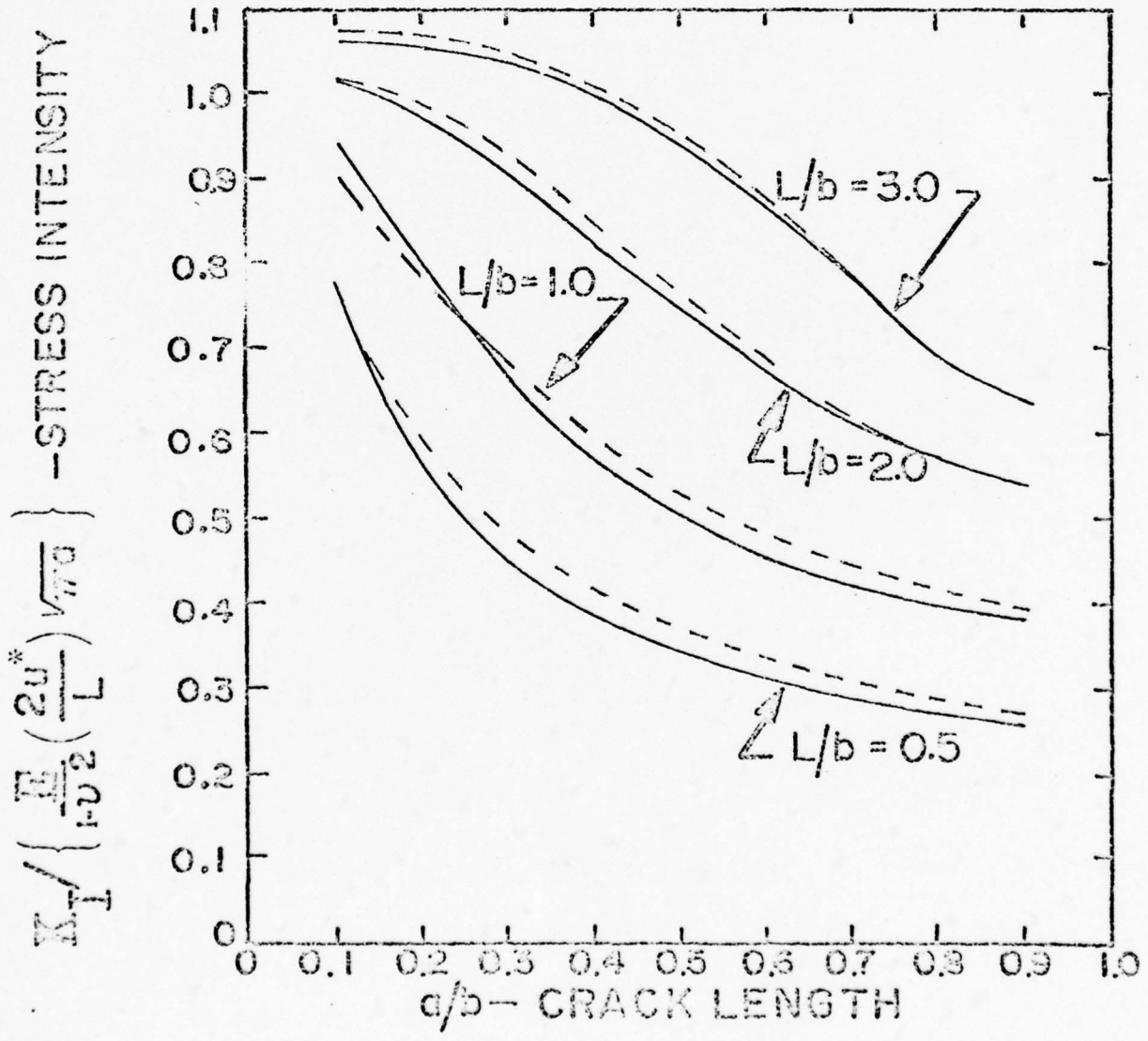

Figure 8 Dimensionless Stress Intensity Factor for Rectangular Plates with Prescribed End Displacements. Transverse constraints — —, No transverse constraints ——— .

This result is compared with the present predictions in Table IV. It should be noted that the normalization is with respect to square root of the plate width, rather than the square root of the crack length, in order to facilitate the comparison. It can be seen that the stress intensity factor in short specimens is very uniform, and close to that given by Equation 41.

Symmetrically located center cracks in strips with prescribed end displacements and free edges have been considered by Bowie[17] and Isida[18]. Stress intensity factors for such problems were also found to be nearly independent of crack length for all but the shortest cracks. Isida's results show that the stress intensity factor for central cracks to be qualitatively the value given by Equation 41 for $L/b < 1$ and $a < c/2$.

Table IV

Dimensionless Stress Intensity Factor

$$K_I / \{ \frac{E}{1-\nu^2} \, (\frac{2u_y^*}{L}) \sqrt{\pi b} \, \}$$

	L/b = 0.5	L/b = 1.0	L/b = 2.0	L/b = 3.0
a/b = 0.1	0.251	0.285	0.295	0.340
a/b = 0.2	0.261	0.352	0.440	0.473
a/b = 0.3	0.261	0.371	0.508	0.573
a/b = 0.4	0.266	0.375	0.534	0.639
a/b = 0.5	0.264	0.375	0.539	0.670
a/b = 0.6	0.264	0.375	0.533	0.673
a/b = 0.7	0.266	0.373	0.523	0.653
a/b = 0.8	0.265	0.370	0.507	0.619
a/b = 0.9	0.260	0.370	0.510	0.606
b = ∞ exact	0.269	0.381	0.538	0.659

VII. Calibration of the Fatigue Crack Life Gauge

It has been proposed[19,20,21] that a thin sheet of metal containing a crack (the gauge) be attached to a structure and the growth of the crack in service monitored as a means of predicting the rate of crack growth in the structure. Both edge cracks[19], and central cracks[20,21] have been suggested, although the edge crack would appear to offer advantages of ease in fabrication. It may also be noted that the observed growth rate of the gauge crack provides a much needed means of quantifying the damaging aspects of the service load spectrum.

The gauge and plate are shown in Figure 9. A perfect bond is assumed on line AB and CD, with gauge and plate not interacting elsewhere. A straight edge crack of length a is assumed to be located on the axis of symmetry of the gauge. It is assumed that the far-field stresses in the plate are a uniaxial tension, σ_p. The state of strain in the plate is uniform if forces generated in the gauge produce negligible deformations in the plate, i.e., if $(E_g t_g / E_p t_p) \ll 1$. In this case, the displacement of AB with respect to O is

$$u_y(x,L/2) = u_y^* = \frac{\sigma_p}{E} \left(\frac{L}{2}\right) \tag{42}$$

Points on the line AB also undergo displacements

$$u_x(x,L/2) = u_x^* = - \nu_p x \frac{\sigma_p}{E} \tag{43}$$

due to the Poisson contraction of the plate to which the gauge is presumed to be perfectly bonded. Here E_p and ν_p are Young's modulus and Poisson's ratio forthe plate, respectively.

These displacements, together with the condition that the edges C_{T_1} and C_{T_2} are free of traction, furnish the boundary conditions for the fatigue crack life gauge. Substituting the displacements into Equation 37

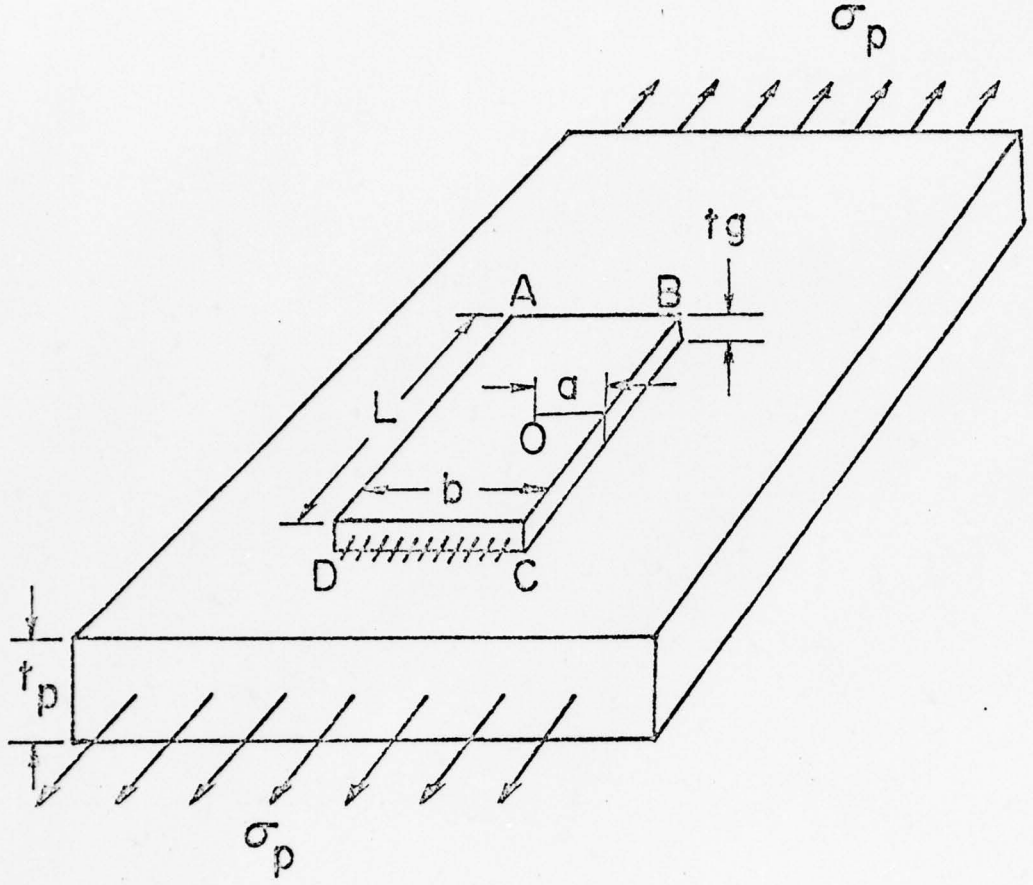

Figure 9 Fatigue Crack Life Gauge

permits the coefficients of the expansion for the stresses and displacements in the gauge to be determined.

Thirty-five elements were again used in the expansion, with the numerical integration of Equation 32 being carried out at 300-400 boundary points. The mode I stress intensity factor is conveniently made dimensionless through division by $\sigma_p\sqrt{\pi a}$, where σ_p is the far field stress intensity in the plate. We find

$$\frac{K_I}{\sigma_p\sqrt{\pi a}} = \frac{K_I}{E_p\left(\frac{2u_y^*}{L}\right)\sqrt{\pi a}} = -\sqrt{2/a}\, d_1 \left(\frac{E_g}{E_p}\right) \tag{44}$$

Dimensionless stress intensity factors for a gauge mounted on a plate are given in Figure 8, where they may be compared with those previously given for the case of complete transverse constraints. A Poisson's ratio of 0.3 was used in these computations. It is of interest to note that the differences are not significant, generally being within the $1-\nu^2$ stiffening effect due to transverse constraints. The Mode I stress intensity factor is essentially determined by the displacements perpendicular to the plane of the crack, and is not sensitive to displacements parallel to the crack plane.

The rigid body motion, allowed through inclusion of a rigid horizontal translation as one of the solutions, was found to have a significant amplitude. The displacement of the crack tip in the direction of the crack can be seen from Figure 10 to be a significant fraction of the end displacement (longitudinal). These displacements may be sufficient to lead to difficulties in attempts to view (photographically) the crack tip while a cyclic test is in progress.

Stress intensity factors for the fatigue crack life gauge with $0.1 \leq a/b \leq 0.9$ are presented in Figure 11 after a different normalization. It

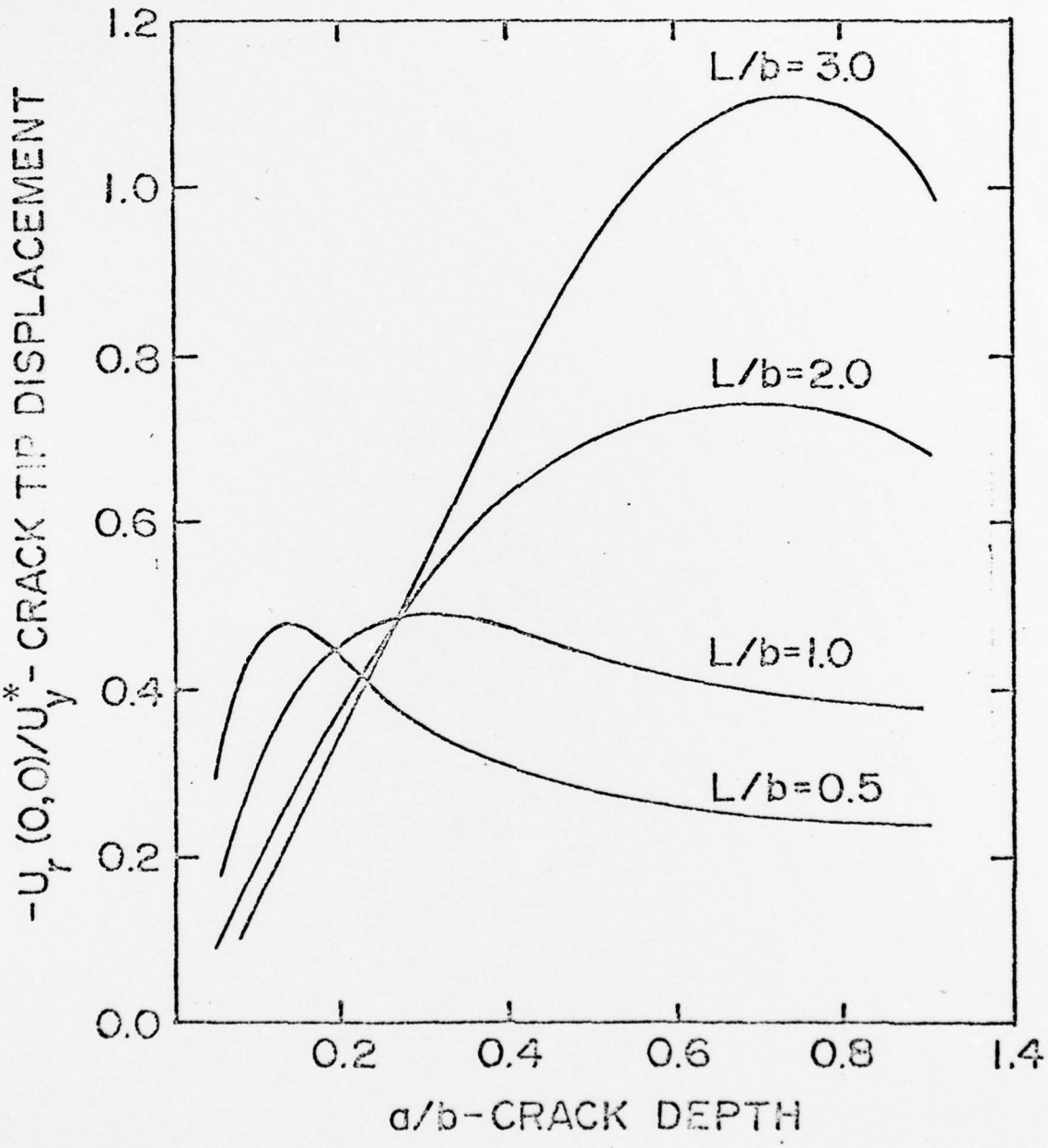

Figure 10 Dimensionless Crack Tip Displacements

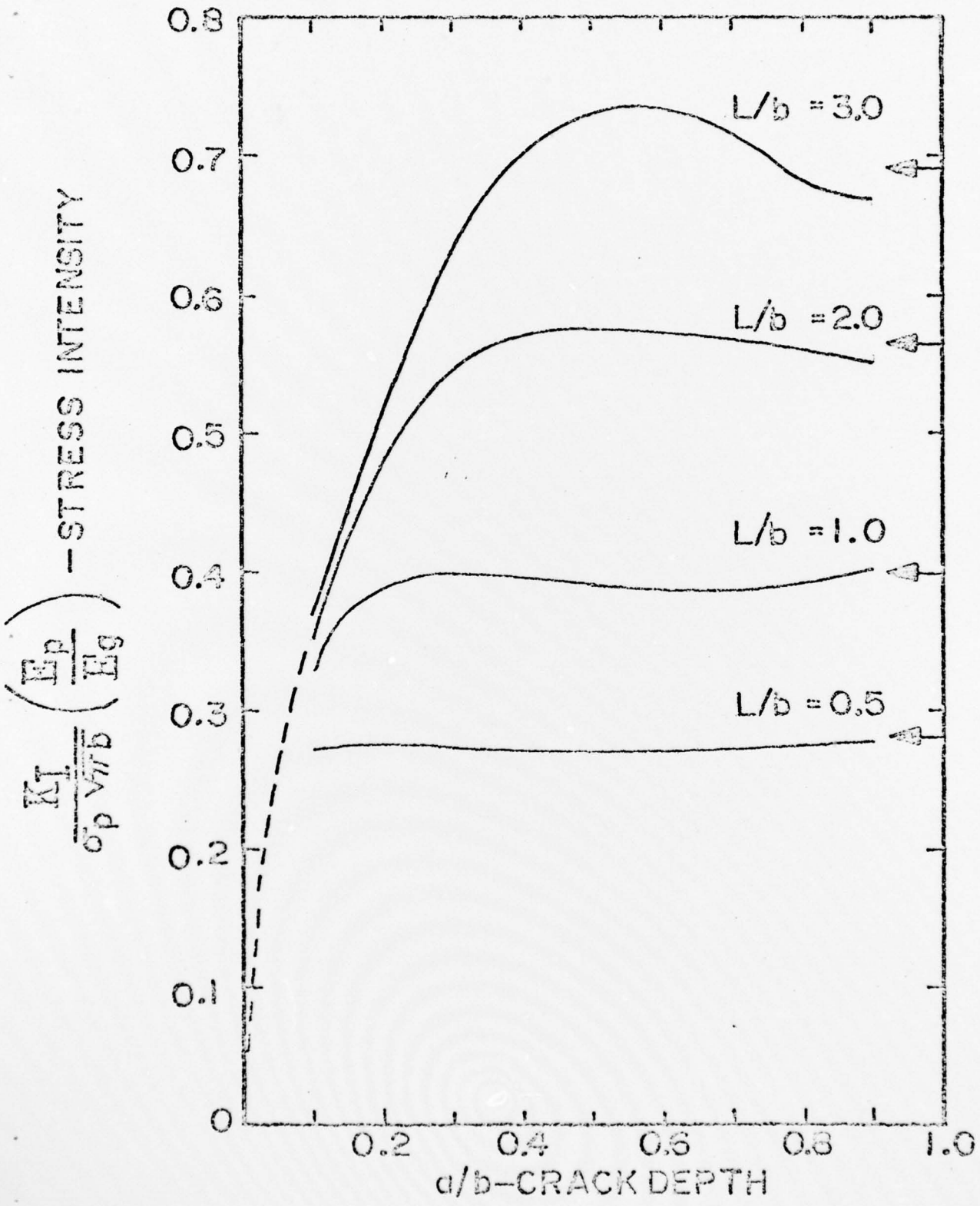

Figure 11 Stress Intensity Factors for Fatigue Crack Life Gauges

can be seen that the stress intensity factor in gauges of low aspect ratio does not vary significantly as the crack length changes. Thus, a gauge crack under constant load will grow at a relatively constant rate, and the rate of change of crack length will provide a measure of instantaneous load spectrum severity which is essentially independent of instantaneous crack length. A constant growth rate under constant load has been observed[19].

Verification of the results may be obtained through consideration of two special cases. Rice[16] has given a stress concentration factor for the centrally cracked infinite strip with

$$u_y(x, \pm L/2) = \pm u_y^* \text{ on } y = \pm L/2$$
$$\tau_{xy}(x, \pm L/2) = 0 \tag{45}$$

as

$$K_I = \sigma\sqrt{L/2} \text{ where} \tag{46}$$

$$\sigma = E_g u_y^* 2/L \tag{47}$$

The boundary conditions for the present problem (Equations 42 and 43) lead to the same energy density at large distances in front of the crack as do those of Equation 45. Consequently, the argument given by Rice may be used to deduce that the stress intensity must be the same. After some manipulation, we find:

$$\frac{K_I}{\sigma_p\sqrt{\pi b}} \left(\frac{E_p}{E_g}\right) = \sqrt{\frac{L}{2\pi b}} \tag{48}$$

It may be seen from Figure 11 that this prediction (arrows) gives surprisingly good agreement for $L/2b < 1$, even though Equation 48 is actually appropriate only for $\lim. \{L/2b \to 0\}$.

A second limiting case is appropriate for $a/b \to 0$ and $a/L \to 0$. In this case, the stress intensity factor should be that of an edge cracked infinite sheet, or

$$\frac{K_I}{\sigma_p\sqrt{\pi b}} \left(\frac{E_p}{E_g}\right) = 1.12\sqrt{\frac{a}{b}} \tag{49}$$

The present results show good agreement with this prediction (dashed curve, Figure 11) for small a/b and long strips.

A properly designed gauge should display neither extremely high, nor extremely low, sensitivity. That is, a gauge length which is entirely consumed during insignificant crack growth in the structure is a poorly designed gauge, as is a gauge which shows little growth during significant (and dangerous) growth in the structure.

At some critical point in the structure a crack of length a_s may be presumed to be growing in accord with the Paris Law, with growth rate dominated by

$$K_{I_S} = \sigma_p \sqrt{\pi a_s}\, M \tag{50}$$

where M is typically greater than 1. In the gage, the crack growth rate is essentially that given by Equation 45, or, for very short cracks, less. Hence,

$$K_{I_g} = \sigma_p \frac{E_g}{E_p} \sqrt{\frac{L}{2}} \tag{51}$$

and we have

$$\frac{K_{I_g}}{K_{I_s}} = \frac{E_g}{E_p} \sqrt{\frac{L}{2\pi a_s}}\, M^* \tag{52}$$

where $M^* < 1$ and decreases as the cracks grow. Thus the initial ratio of gauge crack growth rate to structure crack growth rate can be specified through the selection of guage length and the modulus of the gauge. An initial crack length greater than L/2 has been suggested[19] as being necessary to assure a constant growth rate. The results given as Figure 11 suggest that this criterion may be unnecessarily conservative, and that a ratio $a_o/L > 0.25$ would suffice.

As both cracks grow, the ratio of stress intensity factor in the gauge to that in the structure will diminish, the crack in the structure will begin to grow more rapidly, and the gauge will loose it's sensitivity.

It may therefore be necessary to use more than one crack life gauge on a structure, with one being a durability gauge designed for optimum sensitivity as cracks in the structure approach the length at which crack maintenance is required, and the other gauge, a safety gauge, being designed for optimum sensitivity as cracks in the structure approach the critical crack length.

VIII. DISCUSSION AND CONCLUSIONS

An eigenfunction expansion was used to describe the stresses and displacements in a finite elastic sheet containing a single straight crack which intersects an edge. The set of solutions obtained by Williams for the infinite sheet with crack were used as elements of the expansion, with coefficients chosen by means of the energy principles of elastostatics. The procedure generates an approximate solution which satisfies the field equations everywhere and satisfies the traction free condition on the crack face. When tractions or displacements are prescribed, a stationary value of potential energy or complementary energy is achieved. Such solutions approximate the boundary conditions elsewhere as well as can be accomplished with a given number of terms. The use of Reissner's Principle was found to make possible the construction of solutions when mixed boundary conditions are given.

Although the numerical results do not suggest any difficulties with convergence, the set of functions employed has not been demonstrated to be complete. No multiply-connected domains were considered. The boundary may have arbitrary shape, although it is to be expected that boundaries with re-entrant corners, other than the single crack, might lead to difficulties. No attempt was made to investigate the convergence at singularities introduced by abrupt changes in boundary conditions.

The functions are not orthogonal, in that forces of the pth mode do work in acting through the displacements of the qth mode. Consequently, the array, C, is not diagonal and the addition of elements to the series leads to changes in all coefficients. Convergence was assumed to exist when the addition of terms to the expansion did not change the coefficient

of the first term. The most rapid convergence was found to occur when the boundary points at which the prescribed tractions were approximated were all at about the same distance from the crack tip. Conversely, more terms were found to be required for crack tips near boundaries, and for large aspect ratios. A limitation in the number of terms which can be used, other than one caused by computer storage capacity, was encountered and may limit the degree of accuracy achievable with the method. Eigenfunctions having rapid angular oscillations are required for some geometries, and the large powers of radius which occur in such cases lead to large variations in the magnitudes of the elements of C. This leads to truncation errors in the solution of the system of equations.

For the rectangular sheets considered as examples, these limitations precluded obtaining accuracy results for the stress intensity at crack tips near the boundary, or for long strips. Stress intensity factors for the former case can readily be obtained from the well known results for infinite sheets. Results for long strips with prescribed tractions are not required, as it was found that a strip with an aspect ratio of three is, for all practical purposes, infinite in length. Long strips with prescribed end displacements are somewhat more complex, although a procedure for estimating the stress intensity factor from the stress intensity factor and compliance of short strips is being developed.

Results obtained for the edge cracked rectangular sheet have several important implications for the design of fatigue crack life gauges. These are: (1) The edge cracked configuration appears more desirable than the center cracked configuration, for a shorter initial crack length is necessary in order to achieve a constant stress intensity. This provides more than twice the useful crack growth region. (2) Nearly uniform stress

intensities are achievable in square sheets. (3) It may prove necessary to use gauges which are of a different material than the structure in order to tailor the relative growth rate. Materials with different moduli, as well as crack growth parameters, should be considered. (4) More than one crack gauge may be required on any structure, each having a different sensitivity, as it may not be possible to design a gauge having the desired sensitivity over the entire range of structural crack growth.

Although no anti-symmetric problems were considered, it is to be expected that the formal computation of Mode II stress intensity factors for straight cracks in finite domains can be performed in the same manner. The even functions given in the appendix must then be replaced with the appropriate odd functions, and suitable traction applied.

In addition to its utility in the determination of stress intensity factors, the method can readily be applied to the determination of stresses, strains and displacements in two-dimensional regions having re-entrant corners. For such problems, the appropriate eigen-functions are those corresponding to the eigen-values given by Williams[3] for infinite wedges of vertex angle greater than 180^{o}.

ACKNOWLEDGEMENT

The author is indebted to the Computer Center, Aeronautical Systems Division, Wright-Patterson Air Force Base, for making available the necessary computer facilities required for the calculations reported herein.

Appendix I

The symmetric state of stress, i.e., $\sigma_{\theta\theta}$ and σ_{rr} even in θ, $\sigma_{r\theta}$ odd, is generated by the even stress function

$$\chi_e = (-1)^{n-1} a_{2n-1} r^{n+\frac{1}{2}} \{ - \cos(n-\tfrac{3}{2})\theta + \frac{2n-3}{2n+1} \cos(n+\tfrac{1}{2})\theta \}$$
$$+ (-1)^n a_{2n} r^{n+1} \{ - \cos(n-1)\theta + \cos(n+1)\theta \} \tag{1}$$

The corresponding stresses are found from the usual relationships

$$\sigma_{rr} = \frac{1}{r^2} \frac{\partial^2 \chi_e}{\partial \theta^2} + \frac{1}{r} \frac{\partial \chi_e}{\partial r} \tag{2}$$

$$\sigma_{\theta\theta} = \frac{\partial^2 \chi_e}{\partial r^2} \tag{3}$$

$$\sigma_{r\theta} = - \frac{1}{r} \frac{\partial^2 \chi_e}{\partial r \partial \theta} + \frac{1}{r^2} \frac{\partial \chi_e}{\partial \theta} \tag{4}$$

$$\sigma_{r\theta} = (-1)^{n-1} r^{n-3/2} a_{2n-1} (n-3/2)(n-1/2)\{\sin(n+\tfrac{1}{2})\theta - \sin(n-3/2)\theta\}$$
$$+ (-1)^n r^{n-1} a_{2n}(n)\{(n+1)\sin(n+1)\theta - (n-1)\sin(n-1)\theta\} \tag{5}$$

$$\sigma_{rr} = (-1)^{n-1} r^{n-3/2} a_{2n-1} \cdot \begin{pmatrix} [(n-3/2)^2 - (n+\frac{1}{2})]\cos(n-3/2)\theta \\ - (n-3/2)(n-\frac{1}{2})\cos(n+\frac{1}{2})\theta \end{pmatrix}$$
$$+ (-1)^n r^{n-1} a_{2n} \cdot \begin{pmatrix} [(n-1)^2 - (n+1)]\cos(n-1)\theta \\ - (n+1)n \cos(n+1)\theta \end{pmatrix} \tag{6}$$

$$\sigma_{\theta\theta} = (-1)^{n-1} r^{n-3/2} a_{2n-1} (n+\tfrac{1}{2})(n-\tfrac{1}{2}) \{ \frac{n-3/2}{n+\frac{1}{2}} \cos(n+\tfrac{1}{2})\theta - \cos(n-3/2)\theta \}$$
$$+ (-1)^n r^{n-1} a_{2n}(n)(n+1) \{\cos(n+1)\theta - \cos(n-1)\theta\} \tag{7}$$

It is easily verified that the stresses $\sigma_{\theta\theta}$ and $\sigma_{r\theta}$ vanish on $\theta = \pm \pi$ for all n.

For each ψ_e, we may compute the harmonic function required to generate the displacements by solving the differential equation

$$\nabla^2 \chi_e = \frac{\partial}{\partial r}\left(r \frac{\partial \psi_e}{\partial \theta}\right) . \tag{8}$$

The result is:

$$\psi_e = (-1)^{n-1} \frac{r}{n-\frac{1}{2}}^{n-3/2} a_{2n-1} \cdot \left[\frac{(n-3/2)^2 - (n+\frac{1}{2})^2}{n-3/2} \sin(n-3/2)\theta\right]$$
$$+ (-1)^n \frac{r}{n}^{n-1} a_{2n} \cdot \left[\frac{(n-1)^2 - (n+1)^2}{n-1} \sin(n-1)\theta\right] \tag{9}$$

The corresponding displacements, using Equations 3 and 4 are

$$2\mu u_r = (-1)^{n-1} r^{n-\frac{1}{2}} a_{2n-1} \cdot \begin{pmatrix} [(n+\frac{1}{2}) + \frac{(1-\sigma)}{(n-\frac{1}{2})}\{(n-3/2)^2 - (n-\frac{1}{2})^2\}]\cos(n-3/2)\theta \\ - (n-3/2)\cos(n+\frac{1}{2})\theta \end{pmatrix}$$
$$+ (-1)^n r^m a_{2n} \cdot \begin{pmatrix} [(n+1) + \frac{(1-\sigma)}{n}\{(n-1)^2 - (n+1)^2\}]\cos(n-1)\theta \\ - (n+1)\cos(n+1)\theta \end{pmatrix} \tag{10}$$

and

$$2\mu u_\theta = (-1)^{n-1} r^{n-\frac{1}{2}} a_{2n-1} \cdot \begin{pmatrix} [-(n-3/2) + \frac{(1-\sigma)}{n-\frac{1}{2}}\{(n-3/2)^2 - (n+\frac{1}{2})^2\}]\sin(n-3/2)\theta \\ + (n-3/2)\sin(n+\frac{1}{2})\theta \end{pmatrix}$$
$$+ (-1)^n r^n a_{2n} \cdot \begin{pmatrix} [-(n-1) + \frac{(1-\sigma)}{n}\{(n-1)^2 - (n+1)^2\}]\sin(n-1)\theta \\ + (n+1)\sin(n+1)\theta \end{pmatrix} \tag{11}$$

References

1. Sih, G. C. (Ed) Methods of Analysis and Solutions of Crack Problems, Noordhoff International Publishing Co., Leyden, 1973.

2. Cruse, T. A. and Rizzo, F. J. (Eds) Boundary-Integral Method: Computational Applications in Applied Mechanics, AMD-Vol II, ASME, 1975.

3. Williams, M. L. "Stress Singularities Resulting from Various Boundary Conditions in Angular Corners of Plates in Extension," Journal of Applied Mechanics, Trans. ASME, Vol. 74, December 1952, pp 526-528.

4. Williams, M. L. "On the Stress Distribution at the Base of a Stationary Crack," Journal of Applied Mechanics, Vol. 24, March 1957, pp 109-114.

5. Gross, B., Srawley, J. E. and Brown, W. J. Stress Intensity Factors for a Single-Edge-Notch Tension Specimen by Boundary Collocation of a Stress Function, NASA TN D-2395, August 1964.

6. Gross, B. and Srawley, J. E. Stress Intensity Factors for Single-Edge-Notch Specimens in Bending or Combined Bending and Tension by Boundary Collocation of a Stress Function, NASA TN D-2603, January 1965.

7. Gross, B., Roberts, E. and Srawley, J. E. Elastic Displacements for Various Edge-Cracked Plate Specimens, NASA TN D-4232, November 1967.

8. Hulbert, L. E. and Hopper, A. T. Numerical Analysis of Plane Elastic Regions Containing Holes and Cracks, AFFDL-TR-75-66, Air Force Flight Dynamics Laboratory Technical Report, August 1975.

9. Fung, Y. C. Foundations of Solid Mechanics, Prentice-Hall, New York, 1965, pp 284-306.

10. Benthem, J. P. and Koiter, W. T. "Asymptotic Approximation to Crack Problems," in Methods of Analysis and Solutions of Crack Problems, Noordhoff International Publishing Co., Leyden, 1973, pp 158-160.

11. Tada, Hiroshi, Paris, P., and Irwin, George The Stress Analysis of Cracks Handbook, Dell Research Corporation, Hellertown, PA., 1973, pp 2.10.

12. Bowie, O. L. and Neal, D. M. "Single Edge Crack in Rectangular Tensile Sheet, Journal of Applied Mechanics, Vol. 32, pp 708-709, September 1965.

13. Emery, A. F. and Segedin, C. M. "The Evaluation of Stress Intensity Factors for Cracks Subjected to Tension, Torsion, and Flexure by an Efficient Numerical Technique," Journal of Basic Engineering, Trans. ASME, Vol. 94, Series D, June 1972, pp 387-393.

14. Bowie, O. L. and Neal, D. M. "Stress Intensity Factors for Single Edge Cracks in Rectangular Sheet with Constrained Ends," Technical Report AMRA TR 65-20, U. S. Army Materials Research Agency, Watertown, Mass., August 1965.

15. Bradley, W. B. and Kobayashi, A. S. "Fracture Dynamics - A Photoelastic Investigation," Engineering Fracture Mechanics, Vol. 3, 1971, pp 317-332.

16. Rice, J. R. "Stresses in an Infinite Strip Containing a Semi-Infinite Crack," (Discussion to W. G. Knauss, Vol. 33, p 356, 1966), Trans. ASME, Series E., Journal of Applied Mechanics, Vol. 34, p 248, 1967.

17. Bowie, Oscar "Symmetric Edge Cracks in Tensile Sheet with Constrained Ends," Journal of Applied Mechanics, Vol. 31 , Series E., December 1964, pp 726-728.

18. Isida, M. "Effect of Width and Length on Stress Intensity Factors of Internally Cracked Plates Under Various Boundary Conditions," International Journal of Fracture Mechanics, Vol. 7, No. 3, September 1971, pp 301-316.

19. Smith, Howard W. "Fatigue Damage Indicator," United States Patent No. 3,979,949, September 14, 1976.

20. Grandt, A. F., Crane, R. L. and Gallagher, J. P. A Crack Growth Gage for Assessing Flaw Growth Potential in Structural Components, Proceedings, Fourth International Conference on Fracture, Waterloo, Canada, September 1976.

21. Gallagher, J. P., Grandt, A. F. and Crane, R. L. Tracking Crack Growth Damage at Control Points, AIAA paper no. 77-379, 18th Structures, Structural Dynamics and Materials Conference, San Diego, March 1977.